



# Influence of thermal cycling on structural, optical and electrical properties of vanadium oxide thin films

Xiaochun Wu, Fachun Lai\*, Limei Lin, Yongzeng Li, Lianghui Lin, Yan Qu, Zhigao Huang

School of Physics and Opto-Electronics Technology, Fujian Normal University, Shangsán Road, Cangshan Borough, Fuzhou 350007, PR China

## ARTICLE INFO

### Article history:

Received 19 June 2008

Received in revised form 30 July 2008

Accepted 10 August 2008

Available online 27 August 2008

### Keywords:

Vanadium oxide films

Thermal cycling

Electrical properties

Optical properties

## ABSTRACT

Vanadium oxide films with different thicknesses were deposited on quartz substrates at room temperature by thermal evaporation technique. For investigating the effect of thermal cycling on the properties of the films, the as-deposited films were heated from the room temperature up to 300 °C and then cooled down to the room temperature. The structure and the surface morphology of the samples were studied by X-ray diffraction, Raman spectra and atomic force microscopy. The transmittances of the samples were measured by spectrophotometer. Electrical resistance during thermal cycling was recorded by dual probe method. The experimental results show that the amorphous as-deposited film changes to crystalline structure after thermal cycling. The crystalline film consists of  $V_2O_5$  and a little of  $VO_2$ . A reversible semiconductor–metal phase transition, with decrease of electrical resistance in a factor of  $10^3$ , is observed at temperature about 230 °C during the heating process. An obvious thermal hysteresis in electrical resistance is observed during the thermal cycling. After thermal cycling, the transmittance of the film decreases, but the refractive index and extinction coefficient increase, which are the results of structural change from amorphous to crystalline phase.

© 2008 Elsevier B.V. All rights reserved.

## 1. Introduction

Vanadium oxides including  $V_2O_3$ ,  $V_2O_5$ ,  $V_6O_{13}$ ,  $VO_2$  [1], etc., exhibit a phase transition from the semiconductor phase to the metal phase. This change is accompanied by the important variations of electrical resistivity, optical transmittance and reflectance in the infrared region. The interests in these materials have increased in recent years due to their potential applications in various optoelectronic devices such as catalyst, electronic information displays and color memory devices, smart windows for solar cells, cathode coatings in high-capacity lithium batteries and optical switches [2,3].

The properties of films closely rely on the source materials, deposition techniques and deposition parameters. To obtain specific properties, a lot of techniques have been applied to deposit vanadium oxide thin films, such as reactive sputtering [2,3], pulsed laser deposition [4], reactive-biased target ion beam deposition [5], evaporation [6], chemical vapor deposition [7], and sol–gel process [8]. Among these methods, thermal evaporation is the most common method in producing thin film because it has

many advantages such as stability, reproducibility and high-deposition rate. Moreover, vanadium oxides undergo a semiconductor–metal phase transition when their temperatures increase, which results in the changes of electrical and optical properties. However, there are few reports about the effect of thermal cycling on the properties of the as-deposited vanadium oxide film. Therefore, it is important to investigate the variation of the properties of the film after the thermal cycling in order to assess the practical usefulness of the film.

In this paper, vanadium oxide films with different thicknesses have been deposited on quartz substrates by thermal evaporation technique. The variation of electrical resistance of the film during thermal cycling was studied. The structure, surface morphology and optical properties of the films before and after thermal cycling were investigated.

## 2. Experimental details

Vanadium oxide films were deposited at room temperature on quartz substrates with  $V_2O_5$  (99.95% purity) pellets by a thermal evaporation system. The thicknesses of the films were 200, 300, and 400 nm. The substrates with a diameter of 25 mm were cleaned in acetone and ethanol, then placed in a sample holder and kept at a distance of 30 cm from the evaporation source. The

\* Corresponding author. Tel.: +86 591 22868137; fax: +86 591 22868132.  
E-mail address: [laifc@fjnu.edu.cn](mailto:laifc@fjnu.edu.cn) (F. Lai).

substrate holder was connected to an electric motor to rotate the substrate during the deposition to achieve an uniform film. The base pressure of vacuum chamber was  $3.0 \times 10^{-3}$  Pa and the deposition pressure was  $5.0 \times 10^{-3}$  Pa. Electrical current for evaporation was 120 A. The nominal film thickness was controlled by a quartz crystal thickness monitor.

The as-deposited films were heated in air up to 300 °C from the room temperature and then cooled down to the room temperature, and we define this process as thermal cycling. The crystalline structure of the films was examined by X-ray diffraction (XRD). XRD study was carried out on an X-ray diffractometer (RIGAKU D/MAX2500) with high-intensity Cu K $\alpha$  radiation ( $\lambda = 1.5418$  Å). Raman spectra were taken in the backscattering geometry at room temperature using a RENISHAW 2000 system. An argon ion laser (514.5 nm) was employed as the excitation source. A 50 $\times$  objective was used to focus the laser light on sample surface to a spot of 2.0  $\mu\text{m}^2$ . The surface morphology of films was observed by an atomic force microscopy (AFM) (CSPM 400) under ambient conditions. Scans were taken under the contact mode and over areas of 10  $\mu\text{m} \times 10 \mu\text{m}$  for root mean square (RMS) surface roughness calculation. Electrical resistance of the sample was recorded by the dual probe method using a multimeter (Model 2001 Multimeter, Keithley Instruments Inc.) during the thermal cycling. The temperature of vanadium oxide film was measured by a thermocouple detector located on the film surface. The normal incidence transmittances of the films before and after thermal cycling were recorded by a PerkinElmer Lambda 950 UV/VIS/NIR spectrophotometer in the wavelength range 300–2500 nm. Refractive index and extinction coefficient of the samples were determined from all the normal incidence transmittance data [9].

### 3. Results and discussion

#### 3.1. Structure characterization

XRD results show that all the as-deposited films are amorphous. In this paper, just the pattern of the as-deposited film with 200 nm thickness is given. Fig. 1 shows the XRD patterns of vanadium oxide films with different thicknesses. Fig. 1(a) is the pattern of the as-deposited film with 200 nm thickness. Fig. 1(b), (c) and (d) are the patterns of the films after thermal cycling with thicknesses of 200, 300, and 400 nm, respectively. As can be seen in Fig. 1(a), the as-deposited film exhibits an amorphous structure. The crystalline diffraction peak can be seen obviously in Fig. 1(b)–(d), which confirms that the amorphous as-deposited film changes to be crystalline after the thermal cycling. Comparing the diffraction

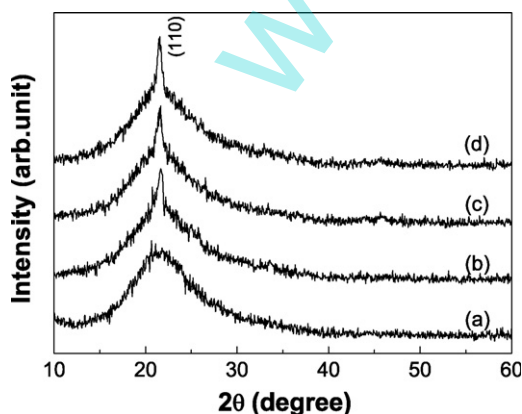


Fig. 1. X-ray diffraction patterns of vanadium oxide films: (a) as-deposited film with 200 nm thickness, and after thermal cycling with different thicknesses (b) 200 nm, (c) 300 nm, and (d) 400 nm.

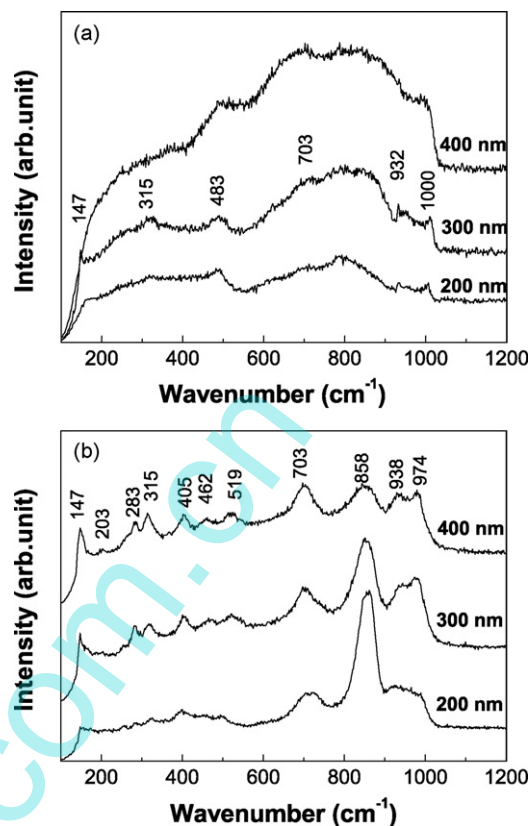


Fig. 2. Raman spectra of vanadium oxide films with different thicknesses: (a) as-deposited and (b) after thermal cycling.

peak position with the data from JCPDS international diffraction data base, it is found that the peak at  $21.6^\circ$  corresponds to (1 1 0) plane of  $\text{V}_2\text{O}_5$  film with orthorhombic structure. This result indicates that the main crystalline phase of the film is  $\text{V}_2\text{O}_5$ .

Fig. 2 shows Raman spectra of the films with different thicknesses before and after thermal cycling. As shown in Fig. 2(a), Raman spectrum in the wavelength range of 100–1200  $\text{cm}^{-1}$  is dominated by the peaks at 147, 315, 483, 703, and 1000  $\text{cm}^{-1}$ , and these peaks are the vibration bands of  $\text{V}_2\text{O}_5$ . The high-frequency Raman peak at 1000  $\text{cm}^{-1}$  corresponds to the terminal oxygen (V=O) stretching mode which results from an unshared oxygen [10]. The vibration mode at about 703  $\text{cm}^{-1}$  is characteristic of the stretching vibration of  $\text{V}_3\text{-O}$  [11]. The two bands at 483 and 315  $\text{cm}^{-1}$  can be related to the stretching frequencies for the V–O–V bonds [12]. The low frequency Raman peak at 147  $\text{cm}^{-1}$  is due to the vibration in a V–O–V atomic chain [3]. The peak at 932  $\text{cm}^{-1}$  is due to the stretching vibration of the  $\text{V}^{4+}=\text{O}$  bond [10]. Therefore, we believe that the as-deposited vanadium oxide films contain a little of  $\text{VO}_2$ .

The Raman spectra in Fig. 2(b) present the following bands: 147, 203, 283, 315, 405, 462, 519, 703, 858, 938, and 974  $\text{cm}^{-1}$ . Comparing Raman spectra (in Fig. 2(a)) of the as-deposited films with those (in Fig. 2(b)) of the films after thermal cycling, it is found that many new peaks in the films after thermal cycling appear, and the peaks at 483, 932, and 1000  $\text{cm}^{-1}$  disappear. The two bands at 938 and 974  $\text{cm}^{-1}$  can be related to the stretching frequencies of the V–O bonds [13]. The signal at 858  $\text{cm}^{-1}$  is due to the O–O mode [14]. The peak at 519  $\text{cm}^{-1}$  is assigned to the triply coordinated oxygen ( $\text{V}_3\text{-O}$ ) stretching mode which results from edge-shared oxygen in common to three pyramids [15]. The two peaks located at 405 and 283  $\text{cm}^{-1}$  are assigned to the bending vibration of the V=O bonds [10]. The remaining two peaks at 462 and 203  $\text{cm}^{-1}$  are

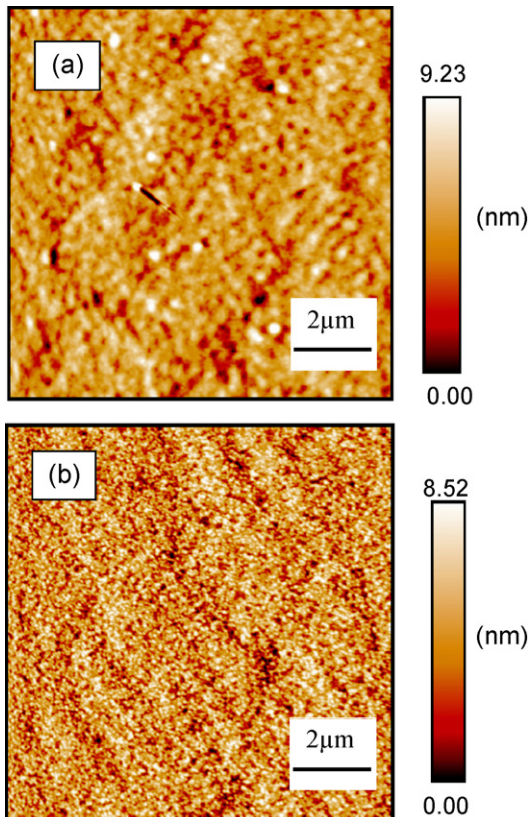


Fig. 3. AFM images of vanadium oxide film with 300 nm thickness: (a) as-deposited and (b) after thermal cycling.

the vibration modes of  $\text{VO}_2$  [12], which also confirms that the films contain some  $\text{VO}_2$ . The peak intensity of the Raman spectra can be affected by the film thickness. The intensity of the peaks at 147, 315, and  $703\text{ cm}^{-1}$  (in Fig. 2(b)) becomes stronger with the increase of film thickness, while the relative intensity of the peak at  $858\text{ cm}^{-1}$  becomes weaker.

### 3.2. Surface morphology

The AFM images of vanadium oxide film with 300 nm thickness before and after thermal cycling are present in Fig. 3. RMS surface roughness and average surface grain size of the films with different thicknesses before and after thermal cycling are shown in Table 1. Not only for the as-deposited film, but also for the films after thermal cycling, both RMS roughness and average surface grain size decrease with the increase in film thickness. When the thickness increases from 200 to 400 nm, RMS roughness of the as-deposited film decreases from 3.7 to 1.3 nm and the average grain size reduces from 154 to 83 nm. Both RMS roughness and average surface grain size for the films after thermal cycling are much smaller than those of the as-deposited films. When the 300 nm thick as-deposited film after thermal cycling, RMS roughness decreases from 1.7 to 1.4 nm and

Table 1

RMS surface roughness and average grain size of vanadium oxide films with different thicknesses

	Thickness (nm)	200	300	400
As-deposited	RMS roughness	3.7	1.7	1.3
	Average grain size	154	123	83
After thermal cycling	RMS roughness	3.0	1.4	1.2
	Average grain size	123	82	73

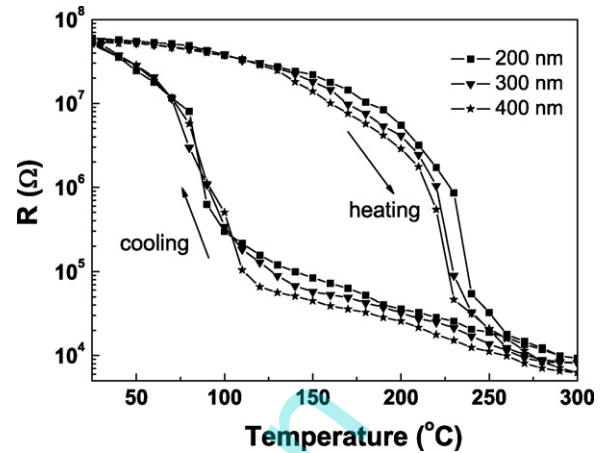


Fig. 4.  $R$ - $T$  curves of vanadium oxide films with different thicknesses.

the average grain size reduces from 123 to 82 nm. The temperature of the film increases in the heating process, which will enhance the mobility of molecules or ions in the film. The movement of molecules or ions may induce the crystallization and the variation of surface morphology of the film [16].

### 3.3. Electrical properties

Fig. 4 shows the variation of the electrical resistance ( $R$ ) of the as-deposited films with different thicknesses as a function of temperature ( $T$ ) during the heating and cooling processes. A sharp decrease and a sudden increase in resistance of the 200-nm film (in Fig. 4) are observed at temperatures in the vicinity of 230 and 90 °C during the heating and cooling processes, respectively. This result shows that three orders of magnitude change occurs in resistance during thermal cycling, which is due to the semiconductor-metal (S-M) transition of the vanadium oxide film. Moreover, we measured the variation of the resistance of the films for the second and the third thermal cycles. The results show that the behavior in variation of resistance is the same with the result of the first cycle. After several thermal cycles, the curves of  $R$ - $T$  of the film did not change, which indicates that the chemical composition of the film does not change.

In order to investigate the switching behavior of resistance accurately, the derivative of the resistance for the heating process was calculated by  $(-d[\log(R)]/dT)$  and the result is shown in Fig. 5. The transition temperature ( $T_t$ ) is defined as the center of the derivative curve and the full width at half maximum (FWHM) is given to describe the abruptness or sharpness of the transition. As indicated in Fig. 5, the  $T_t$  of the 200-nm film is 233 °C and FWHM of the derivative curve is 18 °C. With the thickness increases from 200 to 400 nm, the  $T_t$  diminishes from 233 to 222 °C, and FWHM decreases. The S-M transition temperature of  $\text{VO}_2$  film is about 68 °C [5] and that of  $\text{V}_2\text{O}_5$  film is 257 °C [17]. Youn et al. reported that the  $T_t$  of vanadium oxide increases as  $\text{VO}_2$  changes to  $\text{V}_2\text{O}_5$  [18]. Wei et al. presented that the grain size and crystallization of vanadium oxide film will influence the  $T_t$  [19]. Therefore, we believe that a little  $\text{VO}_2$  in our samples (as discussed in Raman analysis), and the grain size and crystallization of our samples, result in the transition temperature of our samples below 250 °C. In addition, as shown in Fig. 4, the width of hysteresis was defined as the difference between the transition temperatures of heating and cooling processes of the hysteresis loop. When the film thickness increases from 200 to 400 nm, the hysteresis loop width of the film decreases from 140 to 125 °C. This result demonstrates that the  $T_t$  depends on the film thickness, and the thicker film has

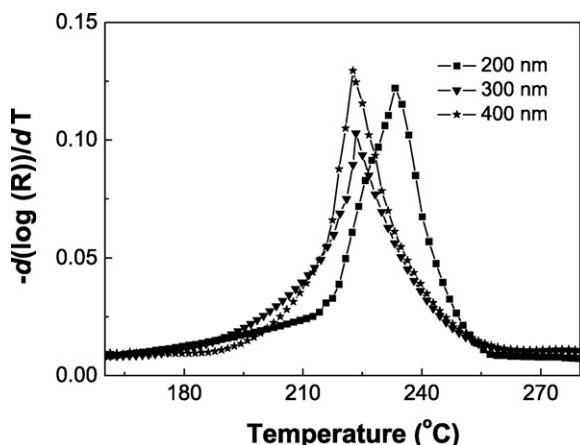


Fig. 5. Derivative of resistance ( $-d[\log(R)]/dT$ ) for the heating process.

the lower  $T_c$ ,  $T_i$  is related to the grain size and crystallization of the film [19]. The films with different thicknesses have different grain size and crystallization (in Fig. 1 and Table 1), which induces the different transition temperature.

### 3.4. Optical properties

After thermal cycling, a color change of the as-deposited films was observed. The color of all the as-deposited films was orange and that of the films after thermal cycling changed to yellowish-black. The final color (at room temperature) was irreversible. The color of the film after the second and the third thermal cycles is the same with that of the film after the first thermal cycle. The change of the structure from amorphous to crystalline phase is irreversible, so the color change of the amorphous as-deposited film after the first thermal cycle is irreversible.

In order to investigate the effect of thermal cycling on the optical properties of the films, transmittances of the samples were measured by a spectrophotometer. As an example, optical transmittance of the 300-nm film is shown in Fig. 6. For the as-deposited film, the interference peaks are lower than the transmittances of the substrate at the corresponding wavelengths, which is due to the absorption and dispersion of vanadium oxide film. Comparing the transmittance of the as-deposited film with that of the film after thermal cycling, it is noted that a sharp decrease in transmittance of the film after thermal cycling, and the average transmittance is lower than 55%. Refractive indices ( $n$ ) and

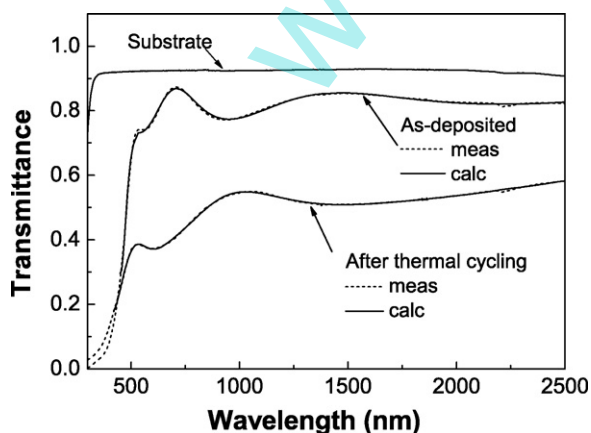


Fig. 6. Measured (dash line) and calculated (solid line) transmittances for vanadium oxide films with 300 nm thickness.

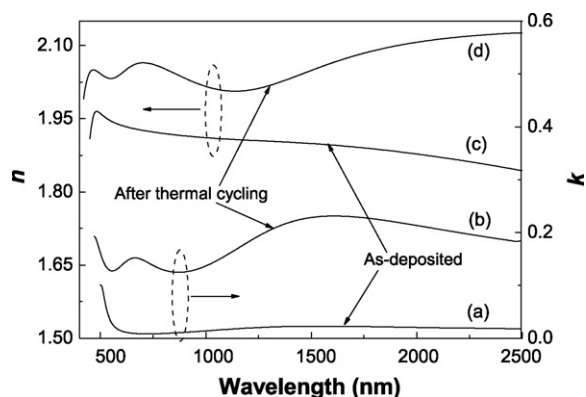


Fig. 7. Extinction coefficient and refractive index as a function of wavelength for vanadium oxide film with 300 nm thickness: as-deposited (a) and (c), and after thermal cycling (b) and (d).

Table 2

Refractive indices ( $n$ ) and extinction coefficients ( $k$ ) of vanadium oxide films with different thicknesses at 600 nm wavelength

Thickness (nm)		200	300	400
As-deposited	$n$	1.88	1.90	1.99
	$k$	0.020	0.014	0.012
After thermal cycling	$n$	2.06	2.08	2.09
	$k$	0.152	0.131	0.096

extinction coefficients ( $k$ ) of the films before and after thermal cycling were calculated from all the transmittance data [9], and the results are shown in Fig. 7. In Fig. 6, the dash curves represent the measured transmittances and the solid curves represent the calculated transmittances. The calculated transmittance was calculated by using the model which combines the Forouhi-Bloomer model and modified Drude model [9]. As shown in Fig. 6, the calculated transmittances are in good agreement with the measured data, which demonstrates the reliability of  $n$  and  $k$ . Fig. 7(c) and (a) are  $n$ - $\lambda$  and  $k$ - $\lambda$  curves of the as-deposited film, respectively. Fig. 7(d) and (b) are  $n$ - $\lambda$  and  $k$ - $\lambda$  curves of the film after thermal cycling, respectively. Fig. 7 shows that the thermal cycling seriously affects  $n$  and  $k$  of the films. Table 2 lists  $n$  and  $k$  of the films before and after thermal cycling with different thicknesses at 600 nm wavelength. In Table 2, for not only the as-deposited films, but also the films after thermal cycling,  $n$  increases and  $k$  decreases with the film thickness increasing. Moreover,  $n$  and  $k$  of all the films after thermal cycling are larger than those of the as-deposited films. For the 300-nm film,  $n$  increases from 1.90 to 2.08 and  $k$  increases from 0.014 to 0.131 at 600 nm wavelength after thermal cycling. This phenomenon can be explained as follows. The density of the film after thermal cycling increased because the structure changes from amorphous to crystalline phase, which resulted in the increase of  $n$  [20]. The surface roughness of the film after thermal cycling is smaller than that of the as-deposited film (in Table 1), so the surface optical scattering decreases. However, the volume optical scattering in the crystalline film after thermal cycling will increase [21], which results in the increase of the total optical scattering and the increase of  $k$ .

### 4. Conclusion

Vanadium oxide films with different thicknesses were deposited on quartz substrates using  $V_2O_5$  pellets by thermal evaporation technique. The as-deposited samples were heated from the room temperature up to 300 °C and then cooled down to the room

temperature. The results show that the amorphous as-deposited films will change to crystalline structure, and the composition of the film after thermal cycling is  $V_2O_5$  and a little of  $VO_2$ . A reversible semiconductor–metal phase transition is observed during thermal cycling, and the change of resistance of the film after thermal cycling is three orders of magnitude. The transition temperature is in the vicinity of 230 °C during the heating process, and the thermal hysteresis loop width is about 130 °C. The color of all the as-deposited films was orange and that of the films after thermal cycling changed to yellowish-black, and this change of color is irreversible. Comparing with the transmittance of the as-deposited film, the transmittance of the film after thermal cycling strongly decreases. Refractive indices and extinction coefficients of the films after thermal cycling are larger than those of the as-deposited films. Additionally, we believe that these variations in optical and electrical properties of vanadium oxide films during the thermal cycling can be applied in further optoelectronic devices.

### Acknowledgments

This work was financially supported by Natural Science Foundation of Fujian Province of China (2007J0317) and Key project of Fujian Provincial Department of Science and Technology (2007H0019). The authors thank Key Laboratory of Optoelectronic Science and Technology for Medicine Ministry of Education for the measurement of spectra.

### References

- [1] F.J. Morin, *Phys. Rev. Lett.* 3 (1959) 34.
- [2] L.J. Meng, R.A. Silva, H.N. Cui, V. Teixeira, M.P.D. Santos, Z. Xu, *Thin Solid Films* 515 (2006) 195.
- [3] S.P. Lim, J.D. Long, S. Xu, K. Ostrikov, *J. Phys. D: Appl. Phys.* 40 (2007) 1085.
- [4] S. Beke, L. Kőrösi, S. Papp, L. Nánai, A. Oszkó, J.G. Kiss, V. Safarov, *Appl. Surf. Sci.* 254 (2007) 1363.
- [5] K.G. West, J. Lu, J. Yu, D. Kirkwood, W. Chen, Y. Pei, J. Claassen, S.A. Wolf, *J. Vac. Sci. Technol. A* 26 (2008) 133.
- [6] A. Kumar, P. Singh, N. Kulkarni, D. Kaur, *Thin Solid Films* 516 (2008) 912.
- [7] C. Piccirillo, R. Binions, I.P. Parkin, *Thin Solid Films* 516 (2008) 1992.
- [8] A. Cremonesi, D. Bersani, P.P. Lottici, Y. Djaoued, R. Brüning, *Thin Solid Films* 515 (2006) 1500.
- [9] F. Lai, L. Lin, R. Gai, Y. Lin, Z. Huang, *Thin Solid Films* 515 (2007) 7387.
- [10] S.H. Lee, H.M. Cheong, M.J. Seong, P. Liu, C.E. Tracy, A. Mascarenhas, J.R. Pitts, S.K. Deb, *Solid State Ionics* 165 (2003) 111.
- [11] R.T.R. Kumar, B. Karunagaran, V.S. Kumar, Y.L. Jeyachandran, D. Mangalaraj, S.K. Narayandass, *Mater. Sci. Semicond. Process.* 6 (2003) 543.
- [12] X.J. Wang, H.D. Li, Y.J. Fei, X. Wang, Y.Y. Xiong, Y.X. Nie, K.A. Feng, *Appl. Surf. Sci.* 177 (2001) 8.
- [13] D. Maniu, T. Iliescu, S. Astilean, *Rom. Rep.* 56 (2004) 419.
- [14] M. Bhattacharjee, M.K. Chaudhuri, P.C. Paul, *Can. J. Chem.* 70 (1992) 2245.
- [15] W. Chen, L. Mai, J. Peng, Q. Xu, Q. Zhu, *J. Solid State Chem.* 177 (2004) 377.
- [16] F. Lai, L. Lin, Z. Huang, R. Gai, Y. Qu, *Appl. Surf. Sci.* 253 (2006) 1801.
- [17] M.F.A. Kuhaili, E.E. Khawaja, D.C. Ingram, S.M.A. Durrani, *Thin Solid Films* 460 (2004) 30.
- [18] D.H. Youn, H.T. Kim, B.G. Chae, Y.J. Hwang, J.W. Lee, S.L. Maeng, K.Y. Kang, *J. Vac. Sci. Technol. A* 22 (2004) 719.
- [19] X.B. Wei, Z.M. Wu, X.D. Xu, T. Wang, J.J. Tang, W.Z. Li, Y.D. Jiang, *J. Phys. D: Appl. Phys.* 41 (2008) 055303.
- [20] X. Wu, F. Lai, L. Lin, J. Lv, B. Zhuang, Q. Yan, Z. Huang, *Appl. Surf. Sci.* 254 (2008) 6455.
- [21] F. Lai, M. Li, H. Wang, H. Hu, X. Wang, J.G. Hou, Y. Song, Y. Jiang, *Thin Solid Films* 488 (2005) 314.